

Longitudinal vortices in unsteady Taylor–Couette flow: solution to a 60-year-old mystery

Ashley P. Willis¹† and Michael J. Burin²

¹Applied Mathematics, School of Mathematical and Physical Sciences, Hicks Building, University of Sheffield, Sheffield S3 7RH, UK

²Department of Physics, California State University, San Marcos, California 92096 USA

(March 2025)

Applying a sufficiently rapid start-stop to the outer cylinder of the Couette–Taylor system, structures approximately aligned with the axis were recorded in the classic work of Coles (1965). These short-lived rolls are oriented perpendicular to the classic Taylor-vortex rolls. In this work we report numerical observation of this instability, guided by a more recent experimental observation. The instability is shown to be related to an inflection in the azimuthal velocity profile, a finding consistent with the experimental observations of its emergence during the deceleration phase. Despite the transient nature of start-stop experiments, we show that the instability can be linked to that of the oscillating boundary layer problem of Stokes. There are several reasons why the instability may have remained elusive, both for experimental observation and for the idealized system. We look in more detail at dependence on the radius ratio for the Taylor–Couette system and find that, in the case where the size of the rolls scales with the gap width, for radius ratios any lower than that used by Coles, $R_i/R_o = 0.874$, the instability is quickly overrun by axisymmetric rolls of Görtler type.

1. Introduction

The nature of the flow of fluid between two rotating cylinders has long played a special role in the study of fluid dynamics and dynamical systems. Taylor (1923) demonstrated that linear stability analysis, using the no-slip condition, could accurately predict the onset of rolls. A large number of distinct flow regimes were soon identified, and Coles (1965)(figure 2 therein) created a summary graphic in the plane defined by the rotation rates of the inner and outer cylinders. This plot included Taylor’s original stability line, above which greater rotation of the inner cylinder rendered the flow unstable to ‘singly periodic flow’ (Taylor-vortices), and catalogued regions of ‘doubly periodic flow’ (wavy Taylor-vortices), in addition to spiral and turbulent flows. Coles was particularly interested in the multiplicity of wavy Taylor vortex states, of various azimuthal wavenumber, and transitions between them. A celebrated version of this diagram, including a greater range of flows, was produced by Andereck *et al.* (1986).

† Email address for correspondence: a.p.willis@sheffield.ac.uk

It is now a little over 100 years since Taylor's landmark paper, 60 years since the classic work of Coles, and the rich dynamical landscape of the Taylor–Couette flow, for the steady rotating case alone, is well recognised.

Multiple flow states for the same rotation rates are not easily represented on a summary graphic, and figure 8 of Coles (1965) is a prime example of this complexity. The addition of time-dependence likewise introduces an extra dimension of complexity, and expeditions in these directions are fewer but significant. Görtler rolls appear when flow encounters a curved surface, and like Taylor-vortex rolls, they are aligned with the direction of the flow and caused by a centrifugal instability. Görtler rolls have been observed to form and eventually evolve into Taylor-vortices for the case of an impulsive start of the inner cylinder, see e.g. Neitzel *et al.* (1995). Studies of an impulsive stop for the outer cylinder include Kohuth & Neitzel (1988); Verschoof *et al.* (2016); Ostilla-Mónico *et al.* (2017); Singh & Prigent (2021), where rolls of many sizes appear and decay, leaving behind the largest scale.

Periodic modulations of the rotation rate of either cylinder have been studied. For example, Ern & Wesfreid (1999) found regimes of both destabilisation and stabilisation, while Youd *et al.* (2003) observed that Taylor-vortex rolls may or may-not reverse the direction of the rolls. Axial oscillations of the inner cylinder have been shown to suppress Taylor instability by Marques & Lopez (1997). In the context of planetary libration, an interesting set of experiments and calculations with modulated rotation rates have been performed, e.g. Noir *et al.* (2010); Lopez & Marques (2011). In all cases discussed above, the same instabilities are manifest, i.e. the appearance of modified Taylor-vortices or Görtler rolls. Other related studies have focused on the effect of surface modulation on a turbulent background state, e.g. Verschoof *et al.* (2018) applied oscillations of the inner cylinder in high Reynolds number experiments and observed how the flow responded to different oscillation rates.

1.1. Experimental observations of longitudinal vortices

Coles (1965) includes an image of a flow, figure 22(o) therein and reproduced in figure 1(a) here, that appears unlike any of those mentioned above. While those flows are dominated by azimuthally aligned rolls that wrap around the cylinder, here the waves are aligned with the axis. In a footnote (p410), Coles describes his method for establishing wavy Taylor vortex flow with a high ‘tangential’ wavenumber, now more commonly referred to as the azimuthal wavenumber m : “*The usual experimental method for establishing a flow with a high tangential wavenumber was to approach the final operating condition from the singly-periodic side [from axisymmetric Taylor rolls] with two cylinders initially rotating in the same direction. A sufficiently fast stop for the outer cylinder then usually led to a flow with a large number of tangential waves, probably as a result of Tollmien instability in the unsteady viscous layer on the wall of the outer cylinder (cf. figure 22(o), plate 12).*” The Tollmien–Schlichting instability is a viscous instability that can occur in a boundary layer flow, such as when a unidirectional flow encounters a flat plate. The rolls that arise within the boundary layer are aligned spanwise to the direction of the flow. In principle, it is possible the sudden-stop could indeed set up a boundary-layer type flow and hence Tollmien instability. However, Coles’ caption to figure 22(o) reads only “*(o) Instability following start-stop motion of outer cylinder.*” The sudden-stop and start-stop experiments are potentially quite different! Unfortunately, no parameters for the start-stop experiment were provided.

More recently, during an experimental campaign to characterize turbulence driven by outer cylinder motion (Burin & Czarnocki 2012), a brief set of start-stop observations were made, revealing what appears to be the same azimuthal instability as described above. See figure 1(b). The instability in this case was observed to arise during the decelerating phase, and for only a narrow gap width ($d = 6.3$ mm and radius ratio $R_i/R_o = 0.97$), although its apparent absence for wider gap widths could be due to visualization shortcomings. A qualitative



Figure 1: (a) Figure 22(o) of Coles (1965), captioned ‘Instability following start-stop motion of outer cylinder.’ (b) Similar observation from the experiments of Burin & Czarnocki (2012)

dependence of the instability wavelength with respect to forcing was observed, with initial acceleration provided by falling weights coupled to the drive system, while mechanical friction provided deceleration. As the acceleration increased, the wavelength increased by a factor of two: from about 1.3 to 2.5 cm, or (approximately) 2 to 4 gap widths. For smaller accelerations the instability was not seen, and for higher ones the turbulence emanating from the end-caps engulfed the central region before the instability could presumably appear. The maximum Reynolds number of the outer cylinder varied in these initial exploratory experiments, although the period and rate of both the acceleration and deceleration phases contain significant uncertainty due to the simple driving mechanism. Nonetheless, this second appearance of the instability in question did reveal that it occurs during the deceleration phase.

To our knowledge, there has been no systematic study of this transitory TC flow state. In this paper, using new simulations alongside these scarce laboratory observations, we aim to clarify when the longitudinal vortices should appear, with respect to the type of motion of the outer cylinder, and to identify the instability mechanism. We show how this particular unsteady flow may be understood within the wider context of unsteady boundary flows, along the way linking Taylor–Coutte flow to a branch of fluid mechanics reaching back to Stokes’ oscillating boundary layer problem.

2. Methods

We consider the flow between concentric cylinders of radius R_i and R_o , where the subscripts indicate the inner and outer cylinders respectively, with rotation rates Ω_i and Ω_o . The radius ratio is denoted by $\eta = R_i/R_o$ and gap width $d = R_o - R_i$. Scales used in the non-dimensionalisation of the governing equations are the gap width d and the viscous diffusion timescale d^2/ν , where ν is the kinematic viscosity, which combine to give a velocity scale ν/d . Quantities in all figures are non-dimensionalised with these scales.

The dimensionless Navier–Stokes equations are

$$\partial_t \mathbf{u} + \mathbf{u} \cdot \nabla \mathbf{u} = -\nabla p + \nabla^2 \mathbf{u}, \quad \nabla \cdot \mathbf{u} = 0. \quad (2.1)$$

Note that the Reynolds numbers, $Re_{i,o} = R_{i,o} \Omega_{i,o} d / \nu$, do not appear in the governing equation but determine the speed of the boundaries: $u_\theta = Re_i$ and $u_\theta = Re_o$ at dimensionless radii $r_i = R_i/d = \eta/(1-\eta)$ and $r_o = R_o/d = r_i + 1$ respectively.

When $Re_{i,o}$ are constant, steady circular-Couette flow is given by

$$\mathbf{u} = V_0(r) \hat{\theta}, \quad V_0(r) = \frac{1}{1+\eta} \left[(Re_o - \eta Re_i) r + \frac{\eta}{(1-\eta)^2} (Re_i - \eta Re_o) \frac{1}{r} \right]. \quad (2.2)$$

To implement the case when time-dependent $\Omega_{i,o}(t)$ imply time-dependent $Re_{i,o}(t)$, we consider the deviation \mathbf{u}' of the velocity field from (2.2) evaluated at each instant, $V_0(r, t) = V_0(r; Re_i(t), Re_o(t))$, i.e.

$$\mathbf{u}(\mathbf{x}, t) = V_0(r, t) \hat{\theta} + \mathbf{u}'(\mathbf{x}, t). \quad (2.3)$$

The field $V_0(r, t)$ is used only in the computations and should be distinguished from the ‘mean profile’ $V(r, t)$, which denotes the azimuthal component of the θ - and z -average of the total flow field \mathbf{u} . The base component of the flow $\mathbf{u} = V_0 \hat{\theta}$ satisfies $\nabla^2 \mathbf{u} = \mathbf{0}$. Substituting (2.3) into (2.1) and using this property, the governing equation for the deviation field \mathbf{u}' can be written

$$(\partial_t - \nabla^2) \mathbf{u}' = \mathbf{u} \times (\nabla \times \mathbf{u}) - \nabla p - (\partial_t V_0) \hat{\theta}, \quad (2.4)$$

subject to $\nabla \cdot \mathbf{u}' = 0$ with boundary conditions $\mathbf{u}' = \mathbf{0}$ at $r = r_{i,o}$. A vector calculus identity has been applied to the advection term to give the rotational form of the governing equation, with the double-cross term on the right. This is slightly easier and less expensive to evaluate numerically.

The code used for time integration of (2.4) is a long-standing variant of the *Openpipeflow* solver (Willis 2017), and modification for this case required only the addition of the forcing term, i.e. the known last term on the right-hand side of (2.4). Periodicity is assumed in the axial dimension over a length $2\pi/\alpha$, and m -fold periodicity can be imposed in the azimuthal dimension. Variables are discretised via a double-Fourier decomposition, and finite differences are used in the radial dimension:

$$a(r_n, \theta, z) = \sum_{|k| < K} \sum_{|m'| < M} A_{km}(r_n) e^{i(\alpha k z + m' m' \theta)}, \quad n = 1, \dots, N. \quad (2.5)$$

Each Fourier mode A_{km} is evaluated at the radial points r_n , which are located at the N extrema the Tchebyshev polynomial $T^{N-1}(x)$ defined on $x = r - r_i \in [0, 1]$. These points are bunched towards the walls within the boundary layers. $N = 100$ for most calculations, while, for linear stability calculations, K and M are only as large as required to capture the first few modes. The Crank–Nicolson method is applied to the diffusion term, while an Euler-predictor and Crank–Nicolson corrector are applied the first and last terms on the right-hand side of (2.4). Via the pressure-Poisson equation, p is used to project the velocity onto the space of divergence-free functions, using an influence-matrix technique to implement the no-slip and divergence-free condition at the wall simultaneously. The difference between the predictor and corrector may be used to control the timestep, but for the calculations here, the timestep is fixed at $\Delta t = 10^{-6}$. (Note that the dimensionless advective timescale $1/|\mathbf{u}| \sim 1/Re_o$.)

The mean profile (θ, z -average) is the component $V(r, t) = u'_{\theta,00} + V_0(r, t)$, where the subscript 00 indicates the $k = m' = 0$ mode in (2.5). In the absence of perturbations, the mean profile is quickly computed by simulating with $K = M = 1$. Eigenvalues, which give the growth rates of linear perturbations to the base flow, are calculated by combining time-integration with Arnoldi iteration. This method applies repeated re-orthogonalisation to the

perturbation via the Gram–Schmidt process, which accelerates convergence to the leading mode, and enables capture of further eigenmodes and eigenvalues. For details, see e.g. Chu *et al.* (2024) §2.2.

3. Results

3.1. Approximation of experiment

The recent experimental observations of longitudinal vortices for a start-stop of the outer cylinder provided the following parameter configuration, which is later rationalised in §3.2. An example video may be found in the supplementary material; 1 second in the video corresponds to approximately 0.024 viscous times d^2/ν .

Instability was observed for the narrow gap, $\eta = 0.97$, and systematic experiments used a weight-and-pully system to start the motion, implying approximately constant acceleration. The outer cylinder was also observed to come to an abrupt halt, suggesting use of a constant decelleration until no motion is reached, rather than say an exponential slow down. Therefore, we begin with a linear ramp up and down in the Reynolds number for the outer cylinder

$$Re_o(t) = \begin{cases} U_1 t/T_1, & 0 \leq t < T_1, \\ U_1 (T_2 - t)/(T_2 - T_1), & T_1 \leq t < T_2, \\ 0, & T_2 \leq t, \end{cases} \quad (3.1)$$

with experimentally-estimated dimensionless parameters $U_1 = 8000$, $T_1 = 0.01$, $T_2 = 0.05$. The inner cylinder is fixed, i.e. $Re_i = 0$. Instability was most frequently observed with an azimuthal wavelength $\lambda \approx 3.5$ (gap widths). Using $\lambda \approx 2\pi r_o/m$, where $r_o = 1/(1 - \eta)$ and m is the rotational symmetry (see (2.5)), implied setting $m = 60$.

Figure 2(a) shows calculations of the azimuthal mean flow profile $V(r, t)$ during the ramp up and ramp down of the outer cylinder. The viscous time-scale d^2/ν was used for the non-dimensionalisation. Similarly, a time scale for the ramp-up stage may be written δ^2/ν , where δ measures how far the change in velocity of the outer boundary is expected to penetrate into the flow. Expressing this in the timescale used for the non-dimensionalisation, we have $\delta^2/\nu = t d^2/\nu$, which rearranges to $\delta/d = \sqrt{t}$. This implies that by the end of the ramp-up stage, at time $t = T_1 = 0.01$, non-zero velocity is expected to penetrate approximately one tenth of the way across the gap, in good agreement with the curve for $t = 0.01$ in figure 2(a). From this time on, the ramp-down is seen in the velocity at the outer boundary, leaving behind a non-zero velocity profile in the interior.

Velocity perturbations are added to $V(r, t)$ that are very small, so that the Fourier modes of the perturbation may be considered to be linearly independent. For the case of axially-aligned rolls, we consider only modes with $k = 0$ in (2.5) so that the calculations are two-dimensional (axially-independent). Small perturbations are added for m' up to 7, but the $m' = 1$ mode is always found to be dominant. Figure 2(b) shows time series of the energy summed over all azimuthally-dependent ($m' \neq 0$) perturbations. It was found that perturbations added at $t = 0$ would not grow substantially, such as the bottom-most curve. Instead, perturbations added at later times during the development of the mean profile were necessary to trigger transient instability. (In the physical experiment, it is perhaps reasonable that some noise is always present, from end conditions at least.) Where a growing mode becomes established, the growth rates appear to be approximately constant for times 0.02-0.04, which is during the decelerating phase, consistent with the appearance of the instability in the experiment.

It is possible in our numerical calculations to freeze the mean profile $V(r, t)$ at a particular time and to calculate the growth rates of infinitesimal disturbances. For this to produce physically reasonable growth rates, it assumes that there is time for the disturbances to grow

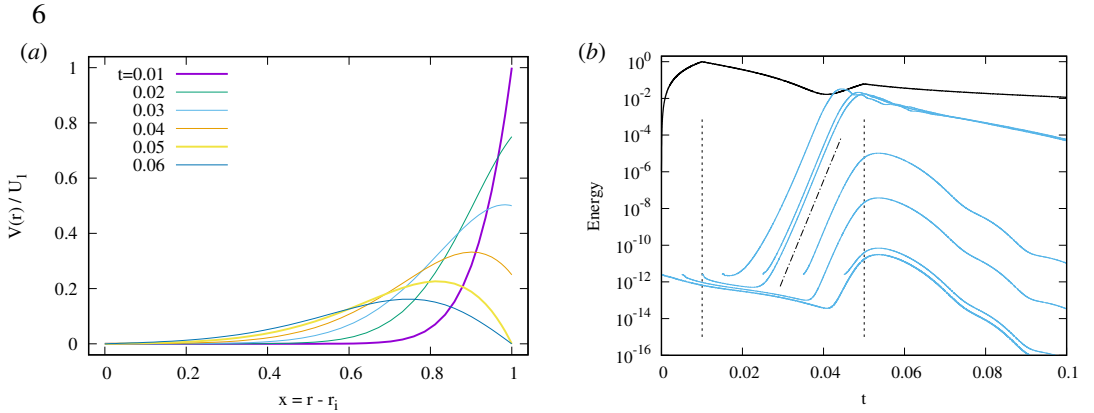


Figure 2: (a) Mean profile during the ramp up of the outer cylinder (from $t = 0$ to $T_1 = 0.01$) and ramp down of the outer cylinder (from $t = T_1$ to $T_2 = 0.05$). (b) Normalised energy of the mean flow, $E_{m=0}(t)/E_{m=0}(T_1)$ (black) and energy of non-axisymmetric ($m \neq 0$) perturbations, $E_{m \neq 0}(t)/E_{m=0}(T_1)$ (blue). Each blue line shows the development of a perturbation introduced at a different time, where the line starts. Vertical lines indicate the times T_1 and T_2 and the slope indicates the growth rate for the wavelength $\lambda \approx 3.5$ at $t = 0.04$ of figure 3.

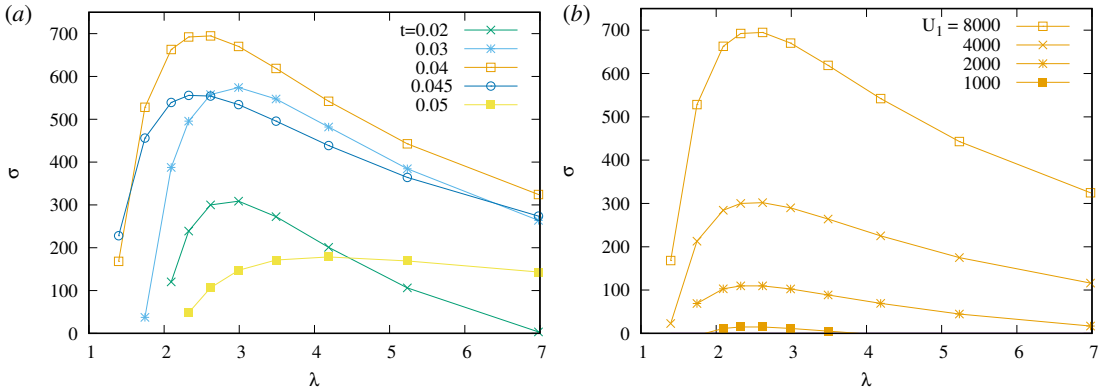


Figure 3: (a) Growth rates σ as a function of azimuthal wavelength λ , assuming frozen mean profiles at the given times. $U_1 = 8000$, $T_1 = 0.01$, $T_2 = 0.05$. (b) Growth rates at $t = 0.04$ changing only U_1 .

substantially more rapidly than changes in the base profile. In figure 2(b), it is seen that perturbations can grow many orders of magnitude in a short time. With this frozen profile assumption, figure 3(a) shows the growth rates of perturbations to the profile as a function of azimuthal wavelength λ at several times. Peak growth is observed at $t = 0.04$ for a wavelength of $\lambda \approx 2.5$, but observe that instability starts earlier at longer wavelengths, $\lambda \approx 3$ for $t = 0.02$ (approximately when growth is first observed), which is a reasonable match to the wavelength observed in the experiment.

For the purely azimuthal base flow $\mathbf{u} = V(r, t)\hat{\theta}$, the nonlinear terms in (2.1) are zero, so that \mathbf{u} can be multiplied through by an arbitrary constant and remains a solution. Therefore, if U_1 is changed without altering T_1 and T_2 , the mean flow is multiplied by a factor but does not change structure. Looking at the time $t = 0.04$ where growth was maximised, figure 3(b) shows that a change in amplitude of the start-stop changes the growth rate of perturbations, but has no noticeable effect on the preferred wavelength of instability.

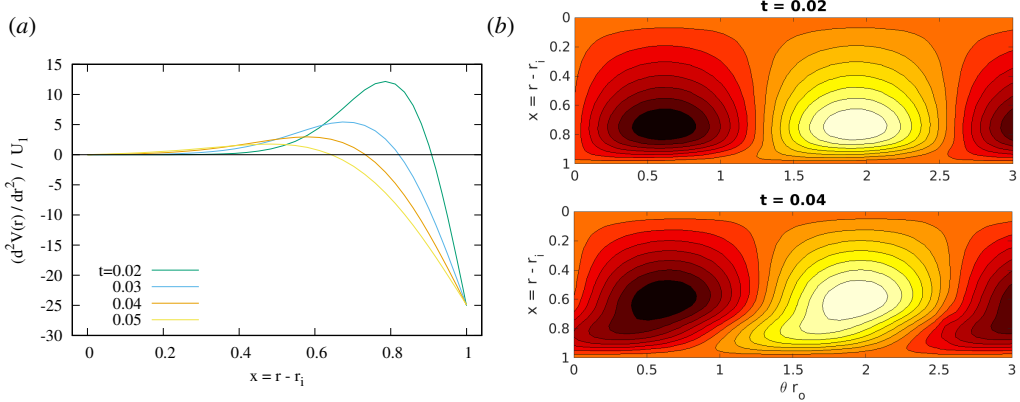


Figure 4: (a) Second derivative of the mean profile for the parameters of figure 2 – roots indicate the location of an inflection point that appears strictly after $T_1 = 0.01$.
 (b) Eigenfunctions of the leading unstable mode with $\lambda \approx 2.6$ at the given times; contours of streamfunction ψ such that eigenfunction $u' = \nabla \times (\psi \hat{z})$.

In the Introduction, it was noted that Coles (1965) had postulated that the rolls ‘probably’ appeared as the result of Tollmien instability, which appears in the boundary layer problem. Acceleration of the boundary sets up a velocity profile of the boundary layer type, but the decelerating phase introduces an inflection point, and it is during this phase that the instability is observed. Figure 4(a) shows the second derivative of the mean profiles at several times, so that the zero of this function tracks the position of an inflection point. Using a wavelength $\lambda \approx 2.6$ ($m = 80$), around the value of theoretical preferred wavelength from figure 3, figure 4(b) shows eigenfunctions at times 0.02 and 0.04 (as viewed from above, looking down the axis of the cylinders). Although the rolls are not centred precisely on the radial location of the inflection point, they are close and move further from the boundary as t increases. Figure 5(a) shows the leading growth rates (of modes with strictly m -periodic dependence) as a function of t . At $t = 0$, the mean flow is zero, so all growth rates are associated with free decay modes. Modes associated with Tollmien instability should arise during the ramp up from $t = 0$ to $t = T_1 = 0.01$, when the mean profile is similar to that for the boundary layer flow. We only see slow adjustment of the growth rates of the free-decay modes, however, during this period. From $t = T_1$, deceleration occurs, the inflection is introduced into the mean profile, and the mode associated with the observed longitudinal vortices quickly appears.

Using the viscous length scale δ introduced in relation to figure 2(a), the accelerating phase may be compared with Stokes’ problem for a flat plate impulsively accelerated to velocity U_0 . A critical value for $Re_I = U_0\delta/\nu$ close to $Re_I = 1485$ has been calculated by Luchini & Bottaro (2001) for the appearance of Tollmien–Schlichting waves. Using the relationship $\delta/d = \sqrt{t}$ and equating U_0 with $R_o\Omega_o$ gives $Re_o = Re_I/\sqrt{t}$. Given that our boundary velocity is only ramped up to U_1 , rather than impulsively started, this provides only a lower bound, $Re_o(t) \geq 1485/\sqrt{t}$, where $\max(Re_o(t)) = U_1$. Within the ramp-up phase, the bound is lowest at $t = T_1 = 0.01$, implying an Re_o greater than 14 850 would be required for Tollmien instability. Calculations with U_1 three times larger at $U_1 = 24\,000$ showed growth rates similar in form (figure 5b), still with no sign of instability before T_1 and instability arising immediately after T_1 . Although Tollmien instability could in principle appear later t , it is unlikely since the velocity profile decays rapidly. Moreover, the appearance of instability at the same time adds extra weight to distinguish it from Tollmien instability, as, when different

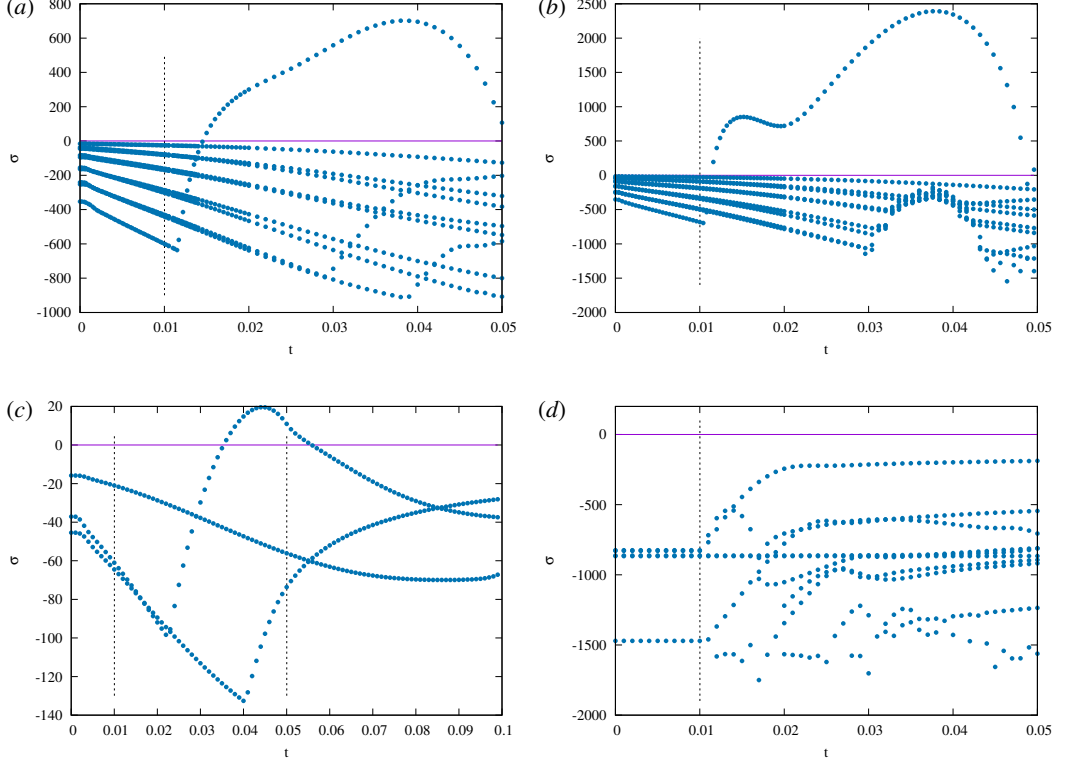


Figure 5: Leading growth rates σ as a function of t for $T_1 = 0.01$, $T_2 = 0.05$, $\lambda \approx 2.6$ ($m = 80$) with (a) $U_1 = 8000$, (b) $U_1 = 24\,000$, and (c) for lower $U_1 = 1000$ shown over a longer period. Vertical lines indicate the times T_1 and T_2 . Only one longitudinal mode goes unstable; all other modes for $t \lesssim 0.03$ connect to the free-decay modes of $t = 0$ when $\mathbf{u} = \mathbf{0}$. (d) Growth rates for the ramp-down of a developed flow: $Re(t) = U_1 = 8000$ for $-\infty < t < T_1$, then $Re(t)$ as before for $t > T_1$.

$Re_o(t)$ are achieved, the bound implies that such instability is expected to arise at a different time t .

As the instability arises during the decelerating phase, it is reasonable to ask whether the accelerating phase is necessary. Figure 5(d) shows the growth rate for the case where the mean flow is developed with $Re(t) = U_1 = 8000$ for all t up until $T_1 = 0.01$, then is followed by the same ramp down to $Re(t) = 0$ at $t = T_2 = 0.05$. All eigenvalues are negative, indicating that both the ramp up and ramp down phases are required for instability.

3.2. Comparison with Stokes' oscillating boundary problem

Stokes found an analytic solution for the flow induced in a semi-infinite body of fluid by a sinusoidal oscillation of an infinite plate. For a plate moving at (dimensional) speed $U = U_0 \cos(\omega t)$, the viscous length scale for the time-varying boundary velocity is often defined $\delta = \sqrt{2\nu/\omega}$. Scaling with U_0 and δ gives a Reynolds number $R^\delta = U_0\delta/\nu$. Von Kerczek & Davis (1974) considered the linear stability of the base flow at each instant for a channel of width d , where the second wall is stationary. For most calculations, the ratio of scales was $\beta = d/\delta = 8$, for which it was shown that the influence of channel width was negligible. The most unstable velocity profile was found to be at time $t = \pi/2$ and that rolls of wavenumber

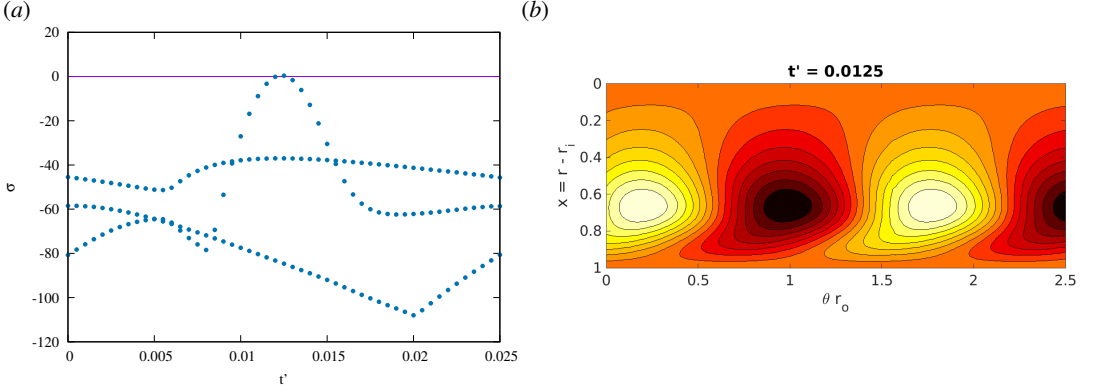


Figure 6: (a) Three leading growth rates for a sinusoidal oscillation of period T as a function of $t' = t - 9.25 T$ in the Taylor-Couette configuration. Parameters for critical U_1 and wavenumber m predicted from Stokes oscillation in a channel. Calculations cover half of the period $T = 0.05$, as the base flow reverses in the second half and eigenvalues repeat.

$Re_o(t)$ is maximum at $t' = 0$ and is zero at $t' = T/4 = 0.0125$. (b) Eigenfunction of the neutral mode.

$\alpha = 0.5$ first go unstable at $R^\delta = 86$. Blondeaux & Vittori (2021) have more recently revisited this analysis for $\beta \rightarrow \infty$, confirming the results of Von Kerczek & Davis (1974). They also examined for which R^δ there is instability in the accelerating phase or over the whole cycle.

To produce the counterpart instability in the Taylor–Couette apparatus, we suppose that the gap for the channel, $d = \beta\delta$, coincides with the Taylor–Couette gap width d , and expect that correspondence will be best for the narrow gap, where curvature terms are small relative to the viscous terms. For the Taylor–Couette system we put $Re_o = U_1 \sin(2\pi t/T)$.

Converting scales from the channel to Taylor–Couette system, we have $\delta = \sqrt{2\nu/\omega} = \sqrt{2\nu(T(d^2/\nu)/(2\pi))} = d \sqrt{T/\pi}$, then using $\beta = d/\delta$ gives $T = \pi/\beta^2$. Maintaining that $\beta = 8$ for the Taylor–Couette system determines a period for the oscillation $T = \pi/8^2 \approx 0.05$. For the velocity amplitude, $U_1(\nu/d) = U_0$ implies $U_1 = U_0 d/\nu = (d/\delta)(U_0 \delta/\nu) = \beta R^\delta$. The critical $R^\delta = 86$ predicts that the amplitude is critical for $U_1 = 688$. The most unstable wavenumber $\alpha = 0.5$ implies $m = 2\pi R_o/\lambda = 2\pi(1/(1-\eta))d/((2\pi/\alpha)\delta)$, which for radius ratio $\eta = 0.97$ and $\beta = 8$ give $m \approx 133$. Using these parameters for the Taylor–Couette setup, figure 6(a) shows the real part of the three leading growth rates for perturbations to frozen mean profiles. The range in t shown corresponds to half a period, as the mean flow is reversed in the second half and has the same growth rates. (Nine oscillations are simulated first to eliminate any transient originating from the initial condition $\mathbf{u}' = \mathbf{0}$ at $t = 0$.) The leading growth rate just touches criticality at the expected time in the cycle, indicating that the prediction derived from the channel calculation of Von Kerczek & Davis (1974) is very good.

Qualitatively, the structure of the growth rates in figure 6(a) is not dissimilar to those of figure 5(c) for the start-stop experiment of §3.1, likewise the structure of the eigenfunction of figure 6(b) is similar to that of figure 4(b) for the start-stop experiment at the later time, when it grows most rapidly. To make an approximately quantitative link, and to a posteriori rationalise the choice of parameters for the start-stop experiment, we make a rough approximation that the linear ramp up and ramp down over a time T_2 corresponds to one half of a sinusoidal oscillation of period $T = 2T_2$. Then, $T = \pi/\beta^2$ for our experiment with $T_2 = 0.05$ implies $\beta = \sqrt{\pi/0.1} \approx 5.6$. This value is not so far from the $\beta = 8$ of

Von Kerczek & Davis (1974), suggesting that, if the instability is of the same nature, the result of §3.1 should not have been substantially influenced by the inner boundary. It should then be possible to predict the most unstable wavelength of the instability from that of the Stokes problem. The wavenumber $\alpha = 0.5$ based on units δ for the channel corresponds to an azimuthal wavelength of $\lambda = (2\pi/\alpha)/\beta \approx 2.2$ in gap widths d . In figure 3 it was found that the peak growth rate occurred for $\lambda \approx 2.5$ in the start-stop experiment, a difference of around 10-20%.

3.3. Dependence on radius ratio

In this section we return to the start-stop problem and consider the case where R_o is fixed and R_i decreases, so that the gap d increases and $\eta = R_i/R_o$ decreases.

If $\Omega_o(t)$ is also unchanged, then the penetration depth δ does not change, and $\beta = d/\delta$ increases. It has been confirmed in calculations that the flow near the outer cylinder is independent of the inner cylinder, and there is no change to the instability (therefore not shown).

If d is increased and $\Omega_o(t)$ scaled such that δ increases proportionately, i.e. $\beta = d/\delta$ is held fixed, then wavelength of the instability will continue to scale with d and the wavenumber m decreases. In this case we expect more influence from the curvature. Conveniently, the dimensionless velocity at the boundary, $V(r_o, t)$, and the time-dependent Reynolds number $Re_o(t)$ are unchanged, as our non-dimensionalisation is already based on the viscous time scale and on d . Only the wavenumber m changes with η : for a change $d \rightarrow \tilde{d}$ and $\eta \rightarrow \tilde{\eta}$, we have $\tilde{m} = m d/\tilde{d} = m (1 - \eta)/(1 - \tilde{\eta})$.

Figure 7 compares the growth of different Fourier modes for $\eta = 0.97, 0.874, 0.8$. The longitudinal vortices are axially independent, $\alpha = 0$, and the non-zero m corresponds to $\lambda \approx 2.6$ for all radius ratios η . The growth of this longitudinal mode is similar for all cases (thick purple line; note the scale on the y-axis). Supposing that the penetration depth δ approximately gives the distance from the outer wall to the centre of a vortex, then it is estimated that the wavelength over a pair of azimuthally independent ($m = 0$) Görtler rolls might be $4\delta/d = 4/\beta$, in units of gap width. For $\beta = 5.6$, the axial wavenumber is then $\alpha = 2.8\pi \approx 8.8$. In figure 7 it is seen that such Görtler modes do not grow for the narrow gap at $\eta = 0.97$, but for $\eta = 0.8$ they are expected to swamp any trace of the longitudinal vortices in a flash. Interestingly, Coles' choice of $\eta = 0.874$ appears to have been a serendipitous one, close to the borderline where both modes might be observed.

4. Conclusions

The figure 22(o) of Coles (1965), captioned “(*o*) instability following start-stop motion of the outer cylinder,” with its longitudinal vortices, has been a bit of a longstanding mystery. When Coles described his procedure for introducing different azimuthal wavenumbers m for wavy Taylor-vortex rolls, he mentioned a sudden-stop that induced a large number of waves, “probably as a result of Tollmien instability,” but referred to the image captioned for a start-stop experiment.

In this work, we have simulated the appearance of longitudinal rolls in the Taylor–Couette system, guided by its unexpected appearance in a more recent experimental campaign (Burin & Czarnocki 2012). We have shown that instability is linked to an inflection point in the mean profile (rather than the Tollmien instability) — despite the transient nature of the start-stop flow, it is possible to link the instability to that of Stokes oscillating boundary problem, which has a Rayleigh instability for sufficiently large Reynolds numbers (Cowley 1987).

There are a number of reasons why the instability may have remained elusive in Taylor–Couette flow. One, of course, is the rich array of other instabilities exhibited by the system,

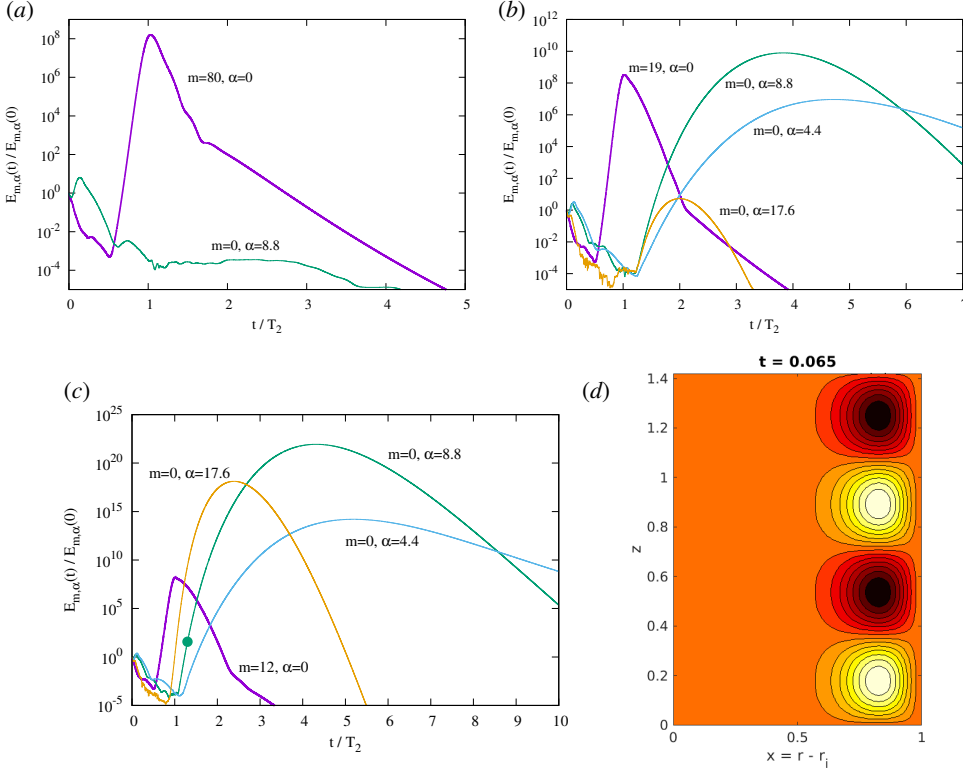


Figure 7: Energy of longitudinal modes ($m \neq 0, \alpha = 0$) and Görtler modes ($m = 0, \alpha \neq 0$) during a start-stop with parameters $U_1 = 8000, T_1 = 0.01, T_2 = 0.05$ at radius ratios (a) $\eta = 0.97$, (b) $\eta = 0.874$, (c) $\eta = 0.8$. For all η , the $m \neq 0$ for longitudinal modes correspond to azimuthal wavelength $\lambda \approx 2.6$.

(d) Görtler mode at time indicated by the point in (c); contours of the Stokes streamfunction ψ , such that $u_r = -(1/r) \partial_z \psi$.

which create other interesting and more manifest diversions. In the recent experiment, longitudinal vortices were only observed for the case $\eta = 0.97$. Guided by this experiment, our parameters suggested a ratio for the viscous scale δ and the gap d of $\beta = d/\delta \approx 5.6$. From the radial extent of the rolls, seen in figure 4(b), it is expected if β is significantly decreased, then without sufficient physical space for the rolls, the instability will be suppressed.

In our calculations where β is fixed while decreasing the radius ratio, i.e. the rolls scale with the gap width, the radius ratio $\eta = 0.874$ of Coles (1965) appears to be around the lower limit at which the instability might be observable. At lower η , the magnitude of curvature terms raises relative to viscous terms, and the instability is almost immediately swamped by centrifugal instability and the formation of Görtler rolls.

It is less obvious why the instability has not been observed for larger β , where the gap d widens but δ is kept the same. This occurs when R_o and $\Omega_o(t)$ are unchanged and only R_i is reduced. Although the instability should be observable in principle, there are practical challenges, and few, if any, of the experiments we have referenced have been looking in the right regime, combining a start-stop or sinusoidal oscillation with a large Reynolds number. For the traditional case of a stationary outer cylinder and steadily rotating inner cylinder, for $\eta = 0.97, 0.874, 0.8$ the critical Reynolds numbers are respectively $Re_i \approx 239, 118, 95$. Here, for a change $d \rightarrow \tilde{d}$, matching the peak boundary velocity gives $\tilde{U}_1(v/\tilde{d}) = U_1(v/d)$, which implies $\tilde{U}_1 = U_1 \tilde{d}/d = U_1(1 - \tilde{\eta})/(1 - \eta)$. For the $U_1 = 8000$, inferred from the

experiment with $\eta = 0.97$ and used in most calculations, this gives $\tilde{U}_1 \approx 3.4 \times 10^4$ at $\eta = 0.874$ and $\tilde{U}_1 \approx 5.3 \times 10^4$ at $\eta = 0.8$. These are the peak values for $Re_o(t)$ for the experiment, and while they are achievable, it is perhaps not usual to be examining linear stability at such large Reynolds numbers.

Another practical difficulty for the case of large β is that, even if the rolls were present, they only occupy a small fraction of the depth that scales like $1/\beta$. This would lead to only a small contrast for traditional visualisation techniques using crystalline platelets.

A final question is the source of perturbations necessary to excite the instability. Endplates for the cylinders naturally break axial independence of the flow. They may lead to Ekmann vortices, and can aid the formation of azimuthally aligned Taylor-vortex rolls. In both Cole's and our experiment pictured in figure 1, turbulence is present at the ends, but often split end plates and other systems are employed to minimise end-effects. If the instability can only be excited from very low level disturbances, in combination with the start-stop being only a transient flow, it is quite possible that in many situations it would not reach sufficient amplitude to be observed.

For the future, with laser-based techniques such as particle image velocimetry (PIV) now more prevalent, such diagnostics may aid further experiments, and possibly lead to more frequent unexpected observations, of this instability over a wider range of radius ratios. Artificial perturbations, such as axially aligned grooves may also enhance the instability, possibly pushing it into regimes where Taylor or Görtler rolls would otherwise take over.

It would also be interesting to revisit whether a signature of the instability may be observed in the presence of turbulence –Verschoof *et al.* (2018) examined turbulent flow with rapid oscillations of the *inner* cylinder, parameterised by the Womersley number $Wo = d\sqrt{\omega/v}$, that correspond to values of $\beta = Wo/\sqrt{2}$ in the range 10.5 to 80.8, commensurate with the instability discussed above. They observed that for shorter modulation periods, the flow responds with a phase delay. Numerical work at large Reynolds numbers has been performed for planar Couette flow by Akhtar & Ostilla-Mónico (2022) with and without rotation, and Akhtar & Ostilla-Mónico (2024) for larger amplitudes and more varied waveforms of the oscillation. They found that modified versions of Stokes' laminar solution persist subject to modified turbulent viscosity, except in the case of cyclonic rotation. It would be interesting to determine whether turbulent mean profiles become unstable to a form of longitudinal instability at very large Reynolds numbers.

Funding. This research received no specific grant from any funding agency, commercial or not-for-profit sectors.

Declaration of interests. The authors report no conflict of interest.

REFERENCES

AKHTAR, M WASY & OSTILLA-MÓNICO, RODOLFO 2022 The effect of modulated driving on non-rotating and rotating turbulent plane couette flow. *Journal of Fluid Mechanics* **943**, A40.

AKHTAR, M WASY & OSTILLA-MÓNICO, RODOLFO 2024 Superposition of system response in modulated turbulent plane couette flow. *Physical review fluids* **9**, 114606–1.

ANDERECK, C DAVID, LIU, SS & SWINNEY, HARRY L 1986 Flow regimes in a circular couette system with independently rotating cylinders. *Journal of Fluid Mechanics* **164**, 155–183.

BLONDEAUX, PAOLO & VITTORI, GIOVANNA 2021 Revisiting the momentary stability analysis of the stokes boundary layer. *Journal of Fluid Mechanics* **919**, A36.

BURIN, M.J. & CZARNOCKI, C.J 2012 Subcritical transition and spiral turbulence in circular couette flow. *Journal of Fluid Mechanics* **709** (1), 106–122.

CHU, SHIJUN, WILLIS, ASHLEY P & MARENSI, ELENA 2024 The minimal seed for transition to convective turbulence in heated pipe flow. *Journal of Fluid Mechanics* **997**, A46.

COLES, DONALD 1965 Transition in circular couette flow. *Journal of Fluid Mechanics* **21** (3), 385–425.

COWLEY, STEPHEN J 1987 High frequency rayleigh instability of stokes layers. In *Stability of Time Dependent and Spatially Varying Flows: Proceedings of the Symposium on the Stability of Time Dependent and Spatially Varying Flows Held August 19–23, 1985, at NASA Langley Research Center, Hampton, Virginia*, pp. 261–275. Springer.

ERN, PATRICIA & WESFREID, JOSE EDUARDO 1999 Flow between time-periodically co-rotating cylinders. *Journal of Fluid Mechanics* **397**, 73–98.

KOHUTH, KERRY RANDALL & NEITZEL, GP 1988 Experiments on the stability of an impulsively-initiated circular couette flow. *Experiments in fluids* **6** (3), 199–208.

LOPEZ, JUAN M & MARQUES, FRANCISCO 2011 Instabilities and inertial waves generated in a librating cylinder. *Journal of Fluid Mechanics* **687**, 171–193.

LUCHINI, PAOLO & BOTTARO, ALESSANDRO 2001 Linear stability and receptivity analyses of the stokes layer produced by an impulsively started plate. *Physics of Fluids* **13** (6), 1668–1678.

MARQUES, FRANCISCO & LOPEZ, JUAN M 1997 Taylor–couette flow with axial oscillations of the inner cylinder: Floquet analysis of the basic flow. *Journal of Fluid Mechanics* **348**, 153–175.

NEITZEL, GP, KIRKCONNELL, CS & LITTLE, LJ 1995 Transient, nonaxisymmetric modes in the instability of unsteady circular couette flow. laboratory and numerical experiments. *Physics of Fluids* **7** (2), 324–334.

NOIR, J, CALKINS, MA, LASBLEIS, M, CANTWELL, J & AURNOU, JM 2010 Experimental study of libration-driven zonal flows in a straight cylinder. *Physics of the Earth and Planetary Interiors* **182** (1–2), 98–106.

OSTILLA-MÓNICO, RODOLFO, ZHU, XIAOJUE, SPANDAN, VAMSI, VERZICCO, ROBERTO & LOHSE, DETLEF 2017 Life stages of wall-bounded decay of taylor–couette turbulence. *Physical Review Fluids* **2** (11), 114601.

SINGH, HARMINDER & PRIGENT, ARNAUD 2021 Turbulence generation and decay in the taylor–couette system due to an abrupt stoppage. *Journal of Fluid Mechanics* **918**, A21.

TAYLOR, GEOFFREY INGRAM 1923 Viii. stability of a viscous liquid contained between two rotating cylinders. *Philosophical Transactions of the Royal Society of London. Series A, Containing Papers of a Mathematical or Physical Character* **223** (605–615), 289–343.

VERSCHOOF, RUBEN A, HUISMAN, SANDER G, VAN DER VEEN, ROELAND CA, SUN, CHAO & LOHSE, DETLEF 2016 Self-similar decay of high reynolds number taylor–couette turbulence. *Physical review fluids* **1** (6), 062402.

VERSCHOOF, RUBEN A, TE NIJENHUIS, ARNE K, HUISMAN, SANDER G, SUN, CHAO & LOHSE, DETLEF 2018 Periodically driven taylor–couette turbulence. *Journal of Fluid Mechanics* **846**, 834–845.

VON KERCZEK, CHRISTIAN & DAVIS, STEPHEN H 1974 Linear stability theory of oscillatory stokes layers. *Journal of Fluid Mechanics* **62** (4), 753–773.

WILLIS, ASHLEY P 2017 The openpipeflow navier–stokes solver. *SoftwareX* **6**, 124–127.

YODD, ANTHONY J, WILLIS, ASHLEY P & BARENGHI, CARLO F 2003 Reversing and non-reversing modulated taylor–couette flow. *Journal of Fluid Mechanics* **487**, 367–376.